Supporting Information

Highly Compact Nano-Channelled Thin Films with Exceptional Thermal Conductivity and Water Pumping for Efficient Solar Steam Generation

Weiwei Wei[a⊥], *Qingbao Guan*[b⊥], *Chuanting You*[c], *Jianyong Yu*[c], *Zhanhui Yuan*[c], *Peirong Qiang*[a], *Chenxin Zhou*[a], *Yi Ren*[d], *Zhengwei You*[b]*, *Fan Zhang*[a]*

[a]School of Chemistry and Chemical Engineering, State key Laboratory of metal matrix composites, Shanghai Electrochemical Energy Devices Research Center, Shanghai Jiao Tong University, Dongchan Road 800, 200240 Shanghai, P. R. China
E-mail: fan-zhang@sjtu.edu.cn (F. Z.)

[b]State Key Laboratory for Modification of Chemical Fibers and Polymer Materials, Shanghai Belt and Road Joint Laboratory of Advanced Fiber and Low-dimension Materials (Donghua University), College of Materials Science and Engineering, Donghua University, Shanghai 201620. China.
E-mail: zyou@dhu.edu.cn (Z. Y.)

[c]College of Materials Science and Engineering, Fujian Agriculture and Forestry University, P. R. China

[d]School of Physical Science and Technology, Shanghai Tech University, 393 Middle Huaxia Road, Shanghai 20210, China

[⊥]These authors contributed equally to this work.

Table of Contents

1. **Experimental section**…….....……...3
2. **Thermodynamic Analysis**…….....……...5
3. **Supplementary Figures**…….....……....6
4. **Supplementary Tables** .....…….……...23

1 Experimental section:

Composite films preparation: The graphene oxide (GO) was prepared via typical Hummers method, and then reduced by hydrazine hydrate to obtain reduced graphene oxide (RGO). In a typical procedure, a solution of CNFs (1wt % in water) was mixed with freshly prepared RGO powder to prepare CNFs/RGO mixed slurry. Afterwards, this CNFs/RGO slurry was fully stirred for 10 min to ensure a completely contact between RGO and CNFs, and then ultrasonically vibricated for 2 hours. It is very crucial that the processes of mixing and ultrasonically have be carried out under 80 ^{o}C in order to enhance the thermal motion of RGO sheet and CNFs fiber. Such performance was repeated for at least 5 times. A homogenous solution was formed. To obtain a more smooth film, we used battery diaphragm (celgard 3501) to replaced traditional (tetrafluoride ethylene) (PTFE) membrane, and slowly filtrated to a composite film with a diameter of 4 cm. Furthermore, the film was naturally dried under ambient conditions for more than one day. The thin-film sample (donated as **CNF@RGO-80**) was peeled readily from the polymer filter. By changing the ratio of RGO/CNFs in 60/40, 70/30 80/20 or 90/10 wt%, a series of GRO/CNFs composite thin films termed as CNF@RGO-60, 70, 80, 90, respectively, were fabricated under the same performance.

The fabrication of solar steam generation device: The composite films of **CNF@RGO-*n*** were cut to a circular flat with a vapor surface area of 5.3066 cm^{-2}. The polystyrene foam (PSF) was also cut to a circular column with surface of 5.3066 cm^{-2} and thickness of 1 cm. This circular column was encased by bibulous paper and foist into a plastic cuvette that was filled with deionized water. The deionized water was pumped up by bibulous paper and soaked the surface of bibulous. The circular flat of C**NF@RGO-*n*** was put on the surface of bibulous paper and soaked by capillarity. This assembly is considered as a simple device for solar steam generation, which utilized the bibulous paper to supply water for the generation surface of **CNF@RGO-*n***. The PSF was used to strut the vapor generation surface meanwhile hinder the transportation of

photothermal energy.

Solar Steam Generation Efficiency Measurement: A standard solar similar (Newport oriel 69907) was used to the steam generation efficiency. The solar steam generation device was placed under the standard similar with different light intensities (1 kW m^{-2}/1sun, 2 kW m^{-2}/2 suns, 3 kW m^{-2}/3 suns) when testing. A k-type thermocouple was used to monitor the upper and low surface temperature under illumination. A calibrated electronic balance was used to measure the mass change during evaporation.

Optical Measurement: optical measure was tested by a UV-vis spectrometer (Lambda 950) from 200 to 2000 nm (PerkinElmer, USA). The sample for test was circular flat with a diameter of 4cm. A bibulous paper was soaked by water and contacted with the circular flat of **CNF@RGO-*n*** to prepare wet sample.

Thermal conductivity measurement: Laser flash method represents a not-contact transient method to measure thermal diffusivity of materials. During testing, an instantaneous laser pulse was used to heat one side of the film, and the response of temperature on the other side was recorded by detector. The Netzsch laser flash apparatus (LFA467) was used for thermal diffusivity measurement. The thermal conductivity k (W m^{-1} K^{-1}) of the samples was then calculated by following formular:

$$k = \alpha \rho C_p \quad (2)$$

where α (mm^2 s^{-1}) is the measured thermal diffusivity along a particular direction, C_p (J g^{-1} K^{-1}) is the heat capacity, and ρ(g cm^{-3}) is the density. The needed heat capacity, C_p, can also be acquired by comparing with standard references lnconel 600 in parallel with thermal diffusivity measurement. The in-plane and crossplane sample were acquire by cutting the wood in different directions.

Adsorption/desorption isothermal measurement: Nitrogen adsorption/desorption isothermal was performed with a Micromeritics ASAP 2020 HD Analyzer at 77 K. Pore

size distribution was estimated based on BJH model. Vapor adsorption/desorption isothermal was performed with a Volume Method Vapor Sorption Analyzer (BSD-PSV) at 25 °C.

The crystallinity of CNFs measurement:

The crystallinity of CNFswas also evaluated by the equation:

$$X_c(\%)=(A_c/A_c+A_a)\times 100 \quad (3)$$

where A_c is the total crystalline area, and A_a is the total amorphous area of the deconvoluted XRD pattern after a subtraction of the background spectra.

2 Thermodynamic Analysis

The distribution of solar energy should follow this equation：

$$E_{Solar} = E_{Vap} + E_{Los} \quad (1)$$

where E_{solar} is the solar energy, the E_{Los} is the energy consumed by heat loss, the E_{vap} is the energy consumed by evaporation which can be written as:

$$E_{vap} = m_1 \times \left[h_v + (T_2 - T_1) \times C_L\right] \quad (2)$$

where h_v is the liquid-vapor phase change (2256 J g^{-1}), and the C_L is heat capacitity of liquid water (4.2 J g^{-1} at 25-100 °C) (*Adv. Funct. Mater.*, **2018**, *28*, 1803266), T_1 is original temperature of block water, T_2 is the stable temperature, m_1 is quantity of evaporating water which can be written as:

$$m_1 = E_{vap} / h_v + (T_2 - T_1) \times C_L \quad (3)$$

The E_{Los} can be calculated as:

$$E_{Los} = Q_{cond} + Q_W \quad (4)$$

where Q_W is the heat loss by heating the excessive water, Q_{cond} is the heat conductive loss from the heat exchange through surface and the heat absorption of skeleton of sample. All of samples exhibit very low heat capacity ($C_{skeleton}$) (the heat capacities of **CNF@RGO-60, 90** are around 0.82 J g^{-1} K^{-1} and 0.72 J g^{-1} K^{-1}, respectively, as depicted in the original vision, page 3, line 7), therefore, the heat absorption from the materials skeletons is always ignored in the previous reports (*Adv. Funct. Mater.*, **2018**, 28, 1803266; *Carbon*, **2019**, 149, 556; *Adv. Mater.*, **2015**, 27, 4302). It is worth noting that the stable temperatures of film's upper surface and bottom surface in each sample are the same (Figure S16). These phenomena are probably due to their unique highly compact porous structure and excellent thermal conductivities of 139 W m^{-1} K^{-1} ~ 614 W m^{-1} K^{-1}, comparable to the recently reported graphene based highly thermal

conductivity materials (*ACS Appl. Mater. Interfaces*, **2011**, *3*, 1325; *Adv. Funct. Mater.*, **2017**, *27*, 1700240). Such high thermal conductivity for such kinds of highly compact porous thin films could allow for quickly transmitting heat over the whole materials. On the other hand, regard to the relatively low the surface areas as compared with their inner specific areas according to BET analysis, the heat losing through their surfaces are too small to be considered in calculation. Thus, Q_{cond} could be ignored in the final calculation. m_2 can be calculated in the following steps:

$$Q_W = (T_2 - T_1) \times m_2 \times C_L \tag{5}$$

where m_2 is the quantity of excessive water. Substituting Eq. (4) into Eq. (5), E_{Los} and m_2 are calculated as:

$$E_{Los} = Q_{cond} + (T_2 - T_1) \times m_2 \times C_L \tag{6}$$

$$m_2 = E_{Los} / (T_2 - T_1) \times C_L \tag{7}$$

Finally, we can calculate the amount of water pumping and loading relative to the photo-thermal conversion as:

$$M = E_{Los} / (T_2 - T_1) \times C_L + E_{vap} / h_v + (T_2 - T_1) \times C_L \tag{8}$$

Where M is total quantity of water pumping and loading.

For **CNF@RGO-60**, the evaporation efficiency (η) is 64% under 1 sun, which means 64 percentage of E_{solar} is used to evaporation and 36 percentage of E_{solar} is lost, thus the M of **CNF@RGO-60** can be written as:

$$M_{60} = E_{solar} \times (0.36 / \Delta T_{60} \times C_L + 0.64 / h_v + \Delta T_{60} \times C_L) \tag{9}$$

ΔT_{60} is difference of the stable temperature (32.8 °C) and the original temperature of block water (~20.4 °C) according to temperature changing curve of **CNF@RGO-60** (Figure S15).

For **CNF@RGO-90**, the evaporation efficiency (η) is 83% under 1 sun, which means 83 percentage of E_{solar} is used to evaporation and 17 percentage of E_{solar} is lost, thus the M of **CNF@RGO-90** can be written as:

$$M_{90} = E_{solar} \times (0.17 / \Delta T_{90} \times C_L + 0.83 / h_v + \Delta T_{90} \times C_L) \tag{10}$$

ΔT_{90} is the difference of the stable temperature (37.1 °C) and the original temperature of block water (~21.3 °C) according to temperature changing curve of **CNF@RGO-90** (Figure S15).

According to Eq. (9) and (10), the ratio of M90/M60 is shown as:

$$M_{90}/M_{60} = (0.17h_v + \Delta T_{90} \times C_L)(\Delta T_{60} \times C_L)(h_v + \Delta T_{60} \times C_L) / (0.36h_v + \Delta T_{60} \times C_L)(\Delta T_{90} \times C_L)(h_v + \Delta T_{90} \times C_L) \tag{11}$$

Accordingly, the ratio of M_{90} to M_{60} could be evaluated as around 0.39, demonstrating that the total water pumping/loading of **CNF@RGO-60** is much large

than that of **CNF@RGO-90**.

3 Supplementary Figures

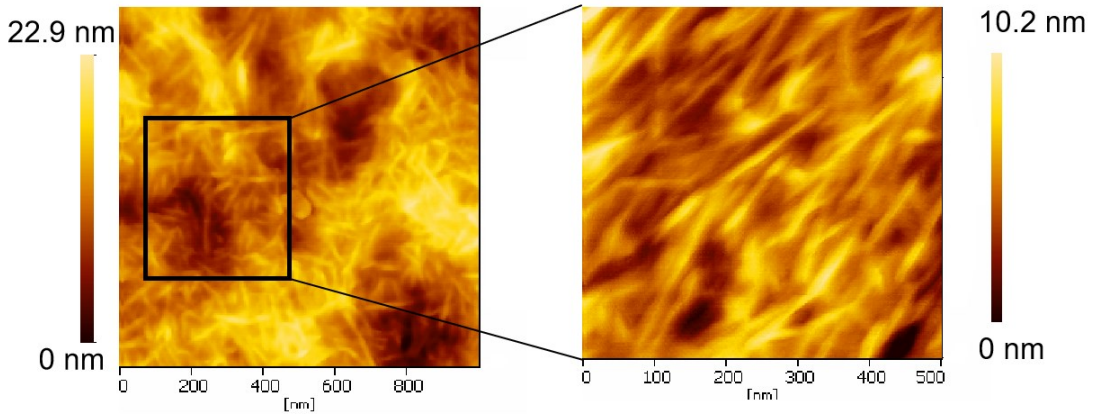

Figure S1. Atomic force microscopy (AFM) images of CNFs used in this work.

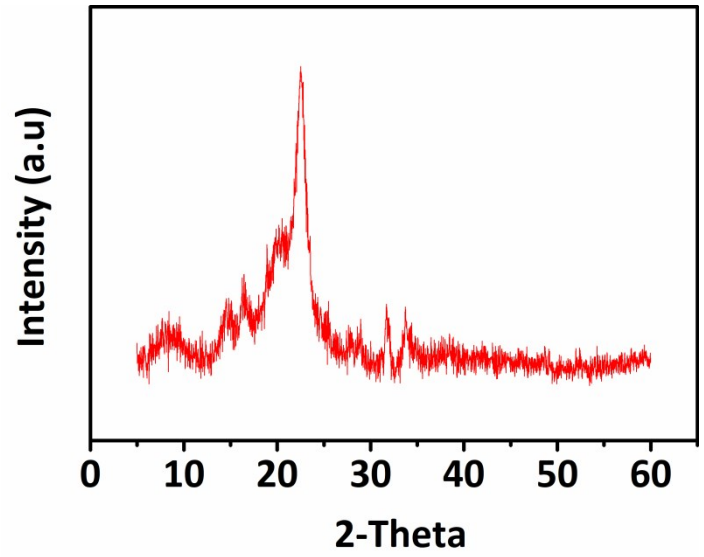

Figure S2. Powder X-ray diffractometer (PXRD) pattern of CNFs.

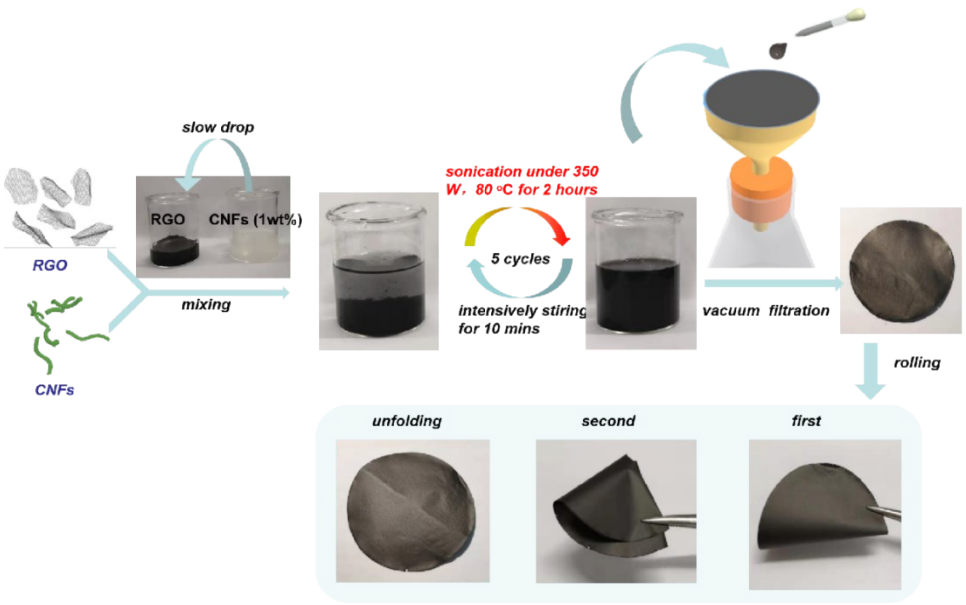

Figure S3. Preparation of **CNF@RGO-*n*** thin films and the photographs of mechanical performances.

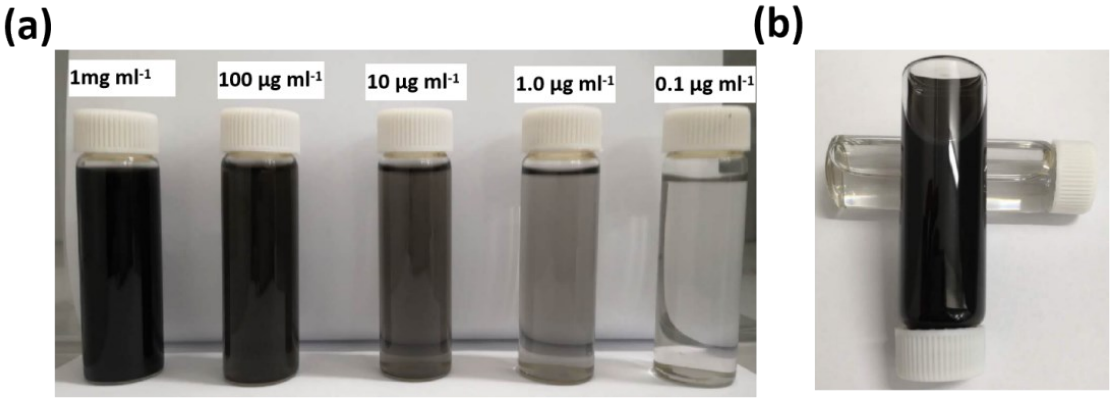

Figure S4. Digital images of (a) CNF/RGO dispersion with different content of RGO (b) CNF/RGO dispersion of 1 mg ml^{-1} after 48 hours.

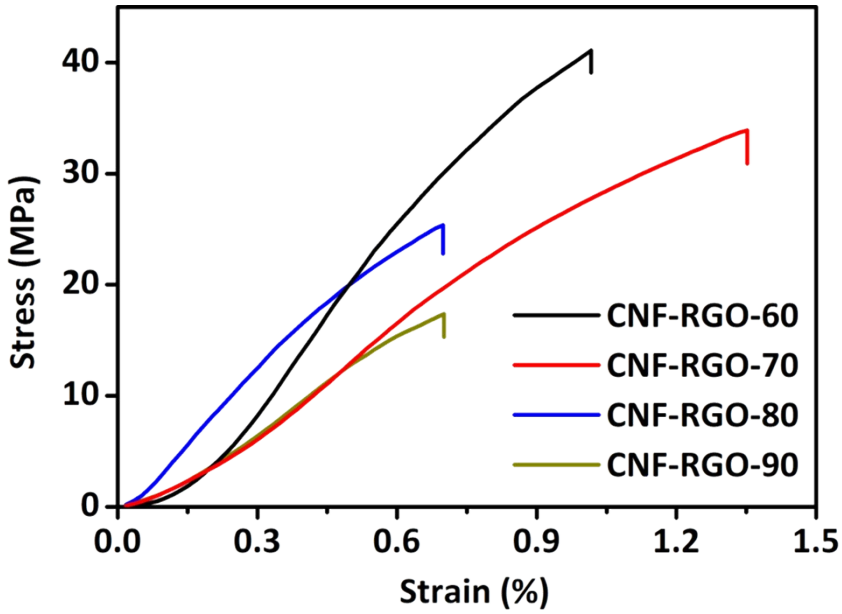

Figure S5. Typical stress-strain curves of **CNF-RGO-*n*.**

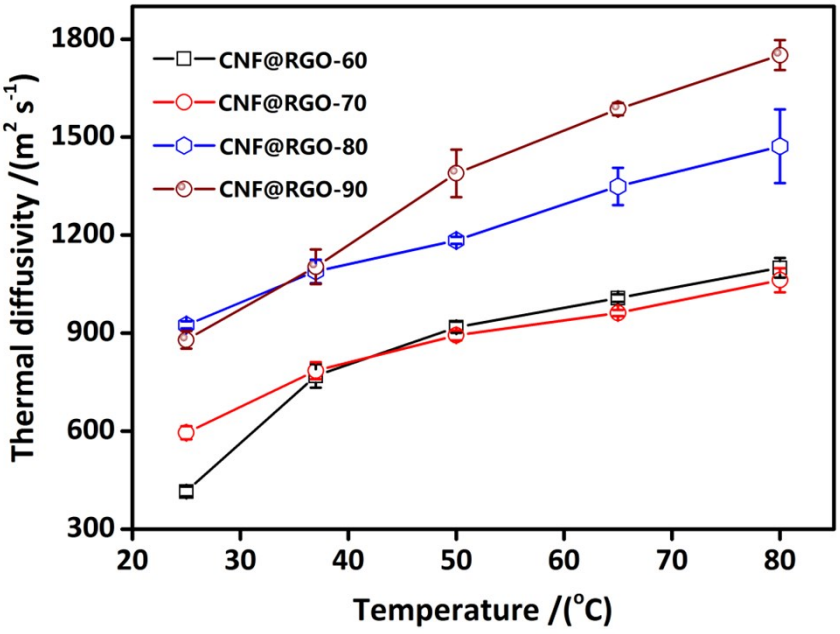

Figure S6. Thermal diffusion coefficient of **CNF@RGO-*n*** under 25~80 °C.

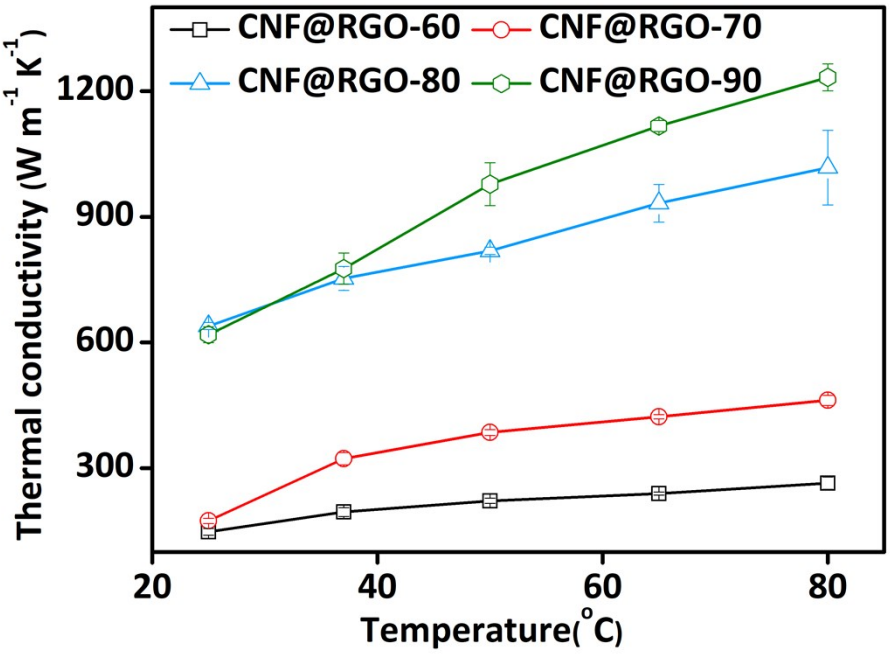

Figure S7.Thermal conductivity of **CNF@RGO-*n*** under 25~80 °C.

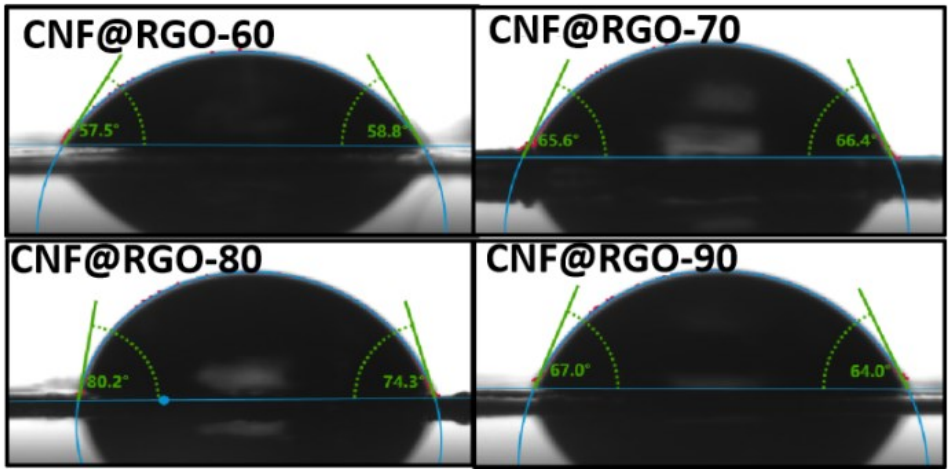

Figure S8. Wettability of sprayed-on the surface of **CNF@RGO-*n***.

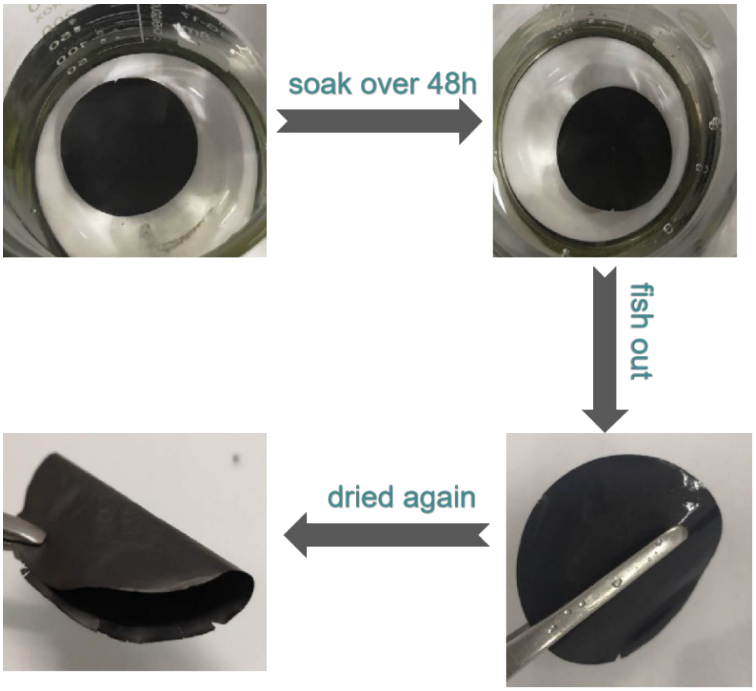

Figure S9. The Digital photographs of CNF@RGO-90 were soaked in water for 48 hours and dried again under 60 ^{o}C.

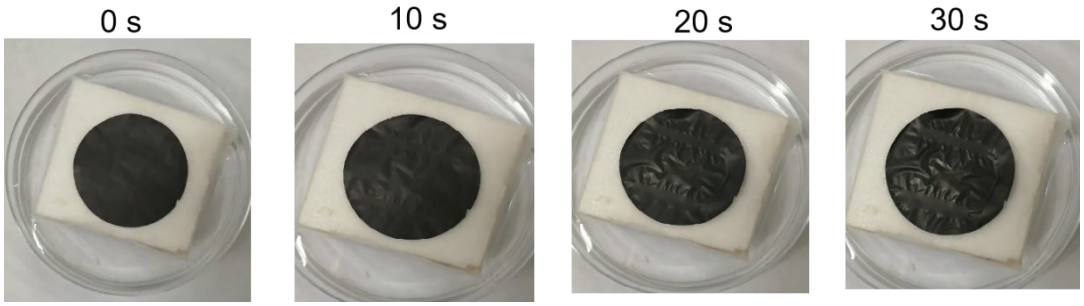

Figure S10. Digital photographs for monitoring the wetting process of **CNF@RGO-90** with a substrate of airlaid paper, which were floated on water.

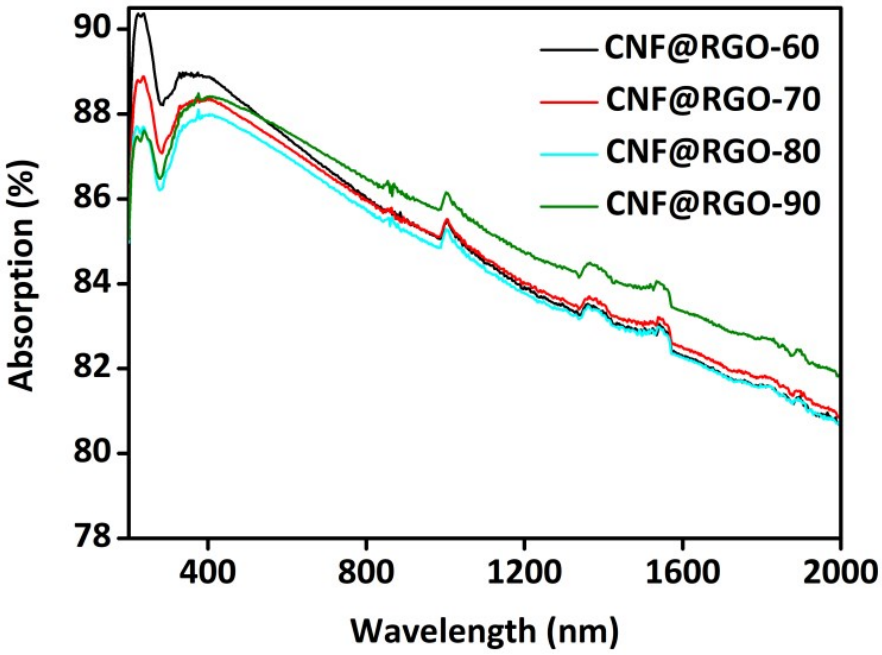

Figure S11. The Absorbance comparison of **CNF@RGO-*n*** under 200-2000nm.

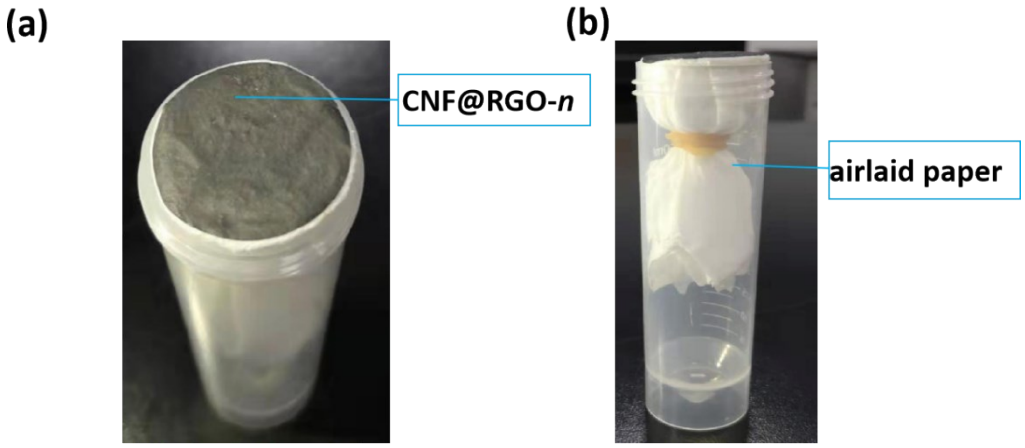

Figure S12. The digital photograph of solar-steam generator： (a) top-view photograph. (b) side-face photograph.

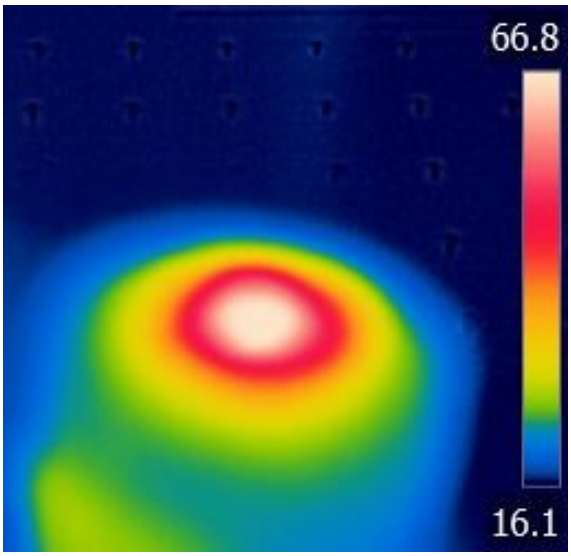

Figure S13. The illustration of distribution between **CNF@RGO-90** and airlaid paper under 3 suns after 600 s.

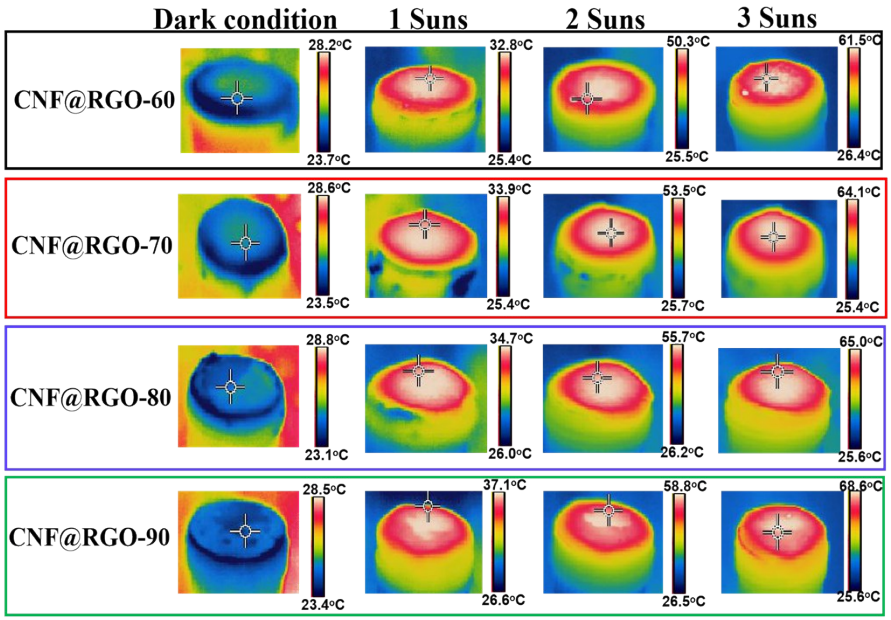

Figure S14 Infrared photo of **CNF@RGO-60，70，80，90** under dark condition and the Infrared photos of 600 S under 1, 2, 3 suns respectively.

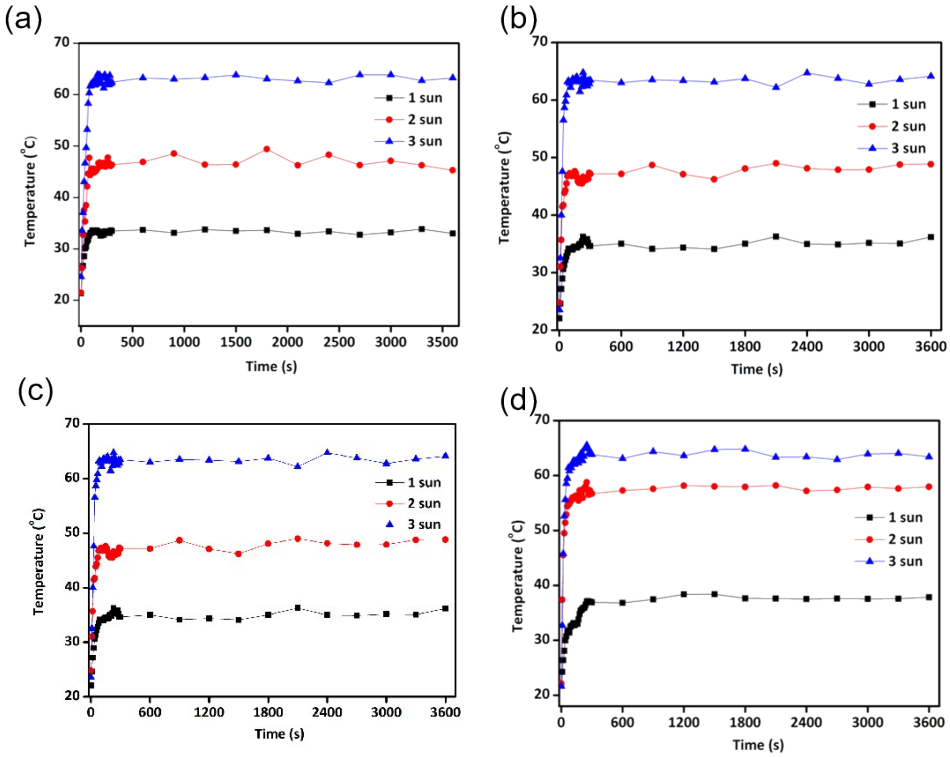

Figure S15 The temperatures of upper surface for **CNF@RGO-60，70，80, 90** under 1, 2, 3suns.

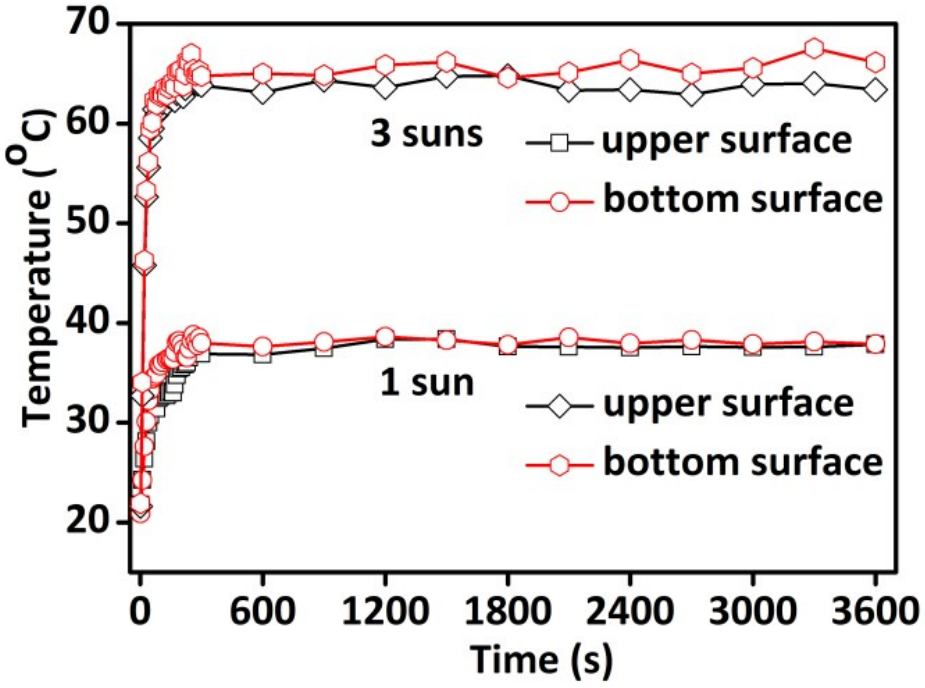

Figure S16. The temperature of upper surface and bottom surface for **CNF@RGO-90** under 1 sun and 3 suns.

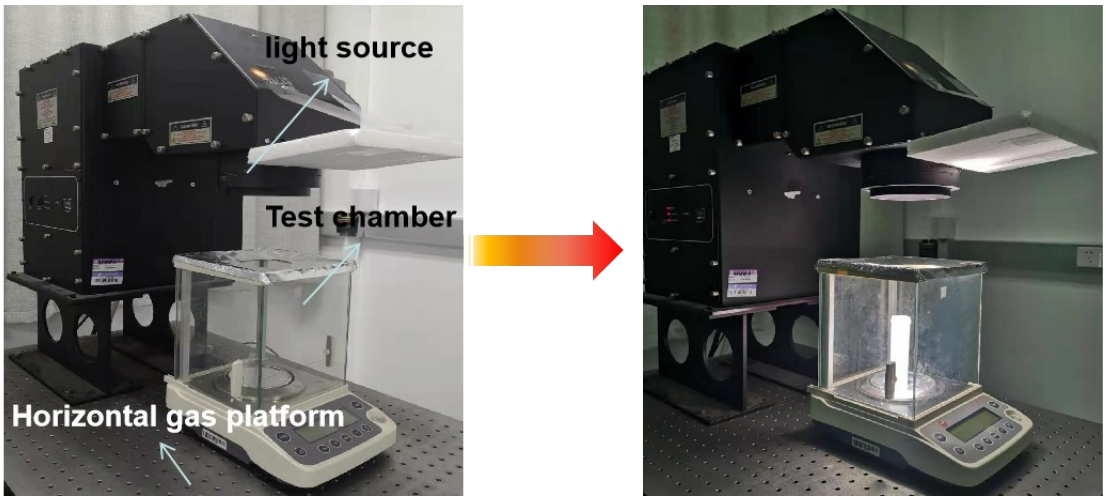

Figure S17. The experimental system of photo-thermal conversion and evaporation rate.

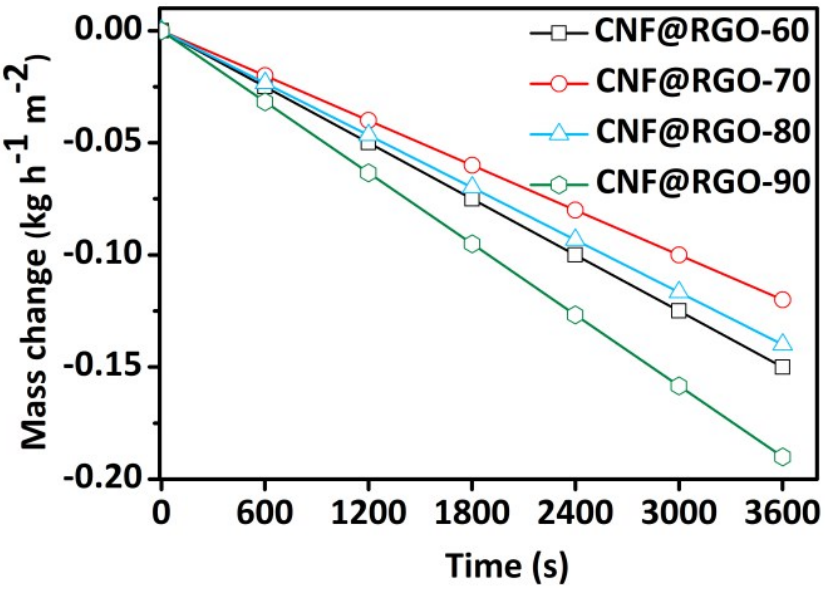

Figure S18. The dark evaporation rate of **CNF@RGO-*n*** at ~25 °C and a relative humidity of 50-55%.

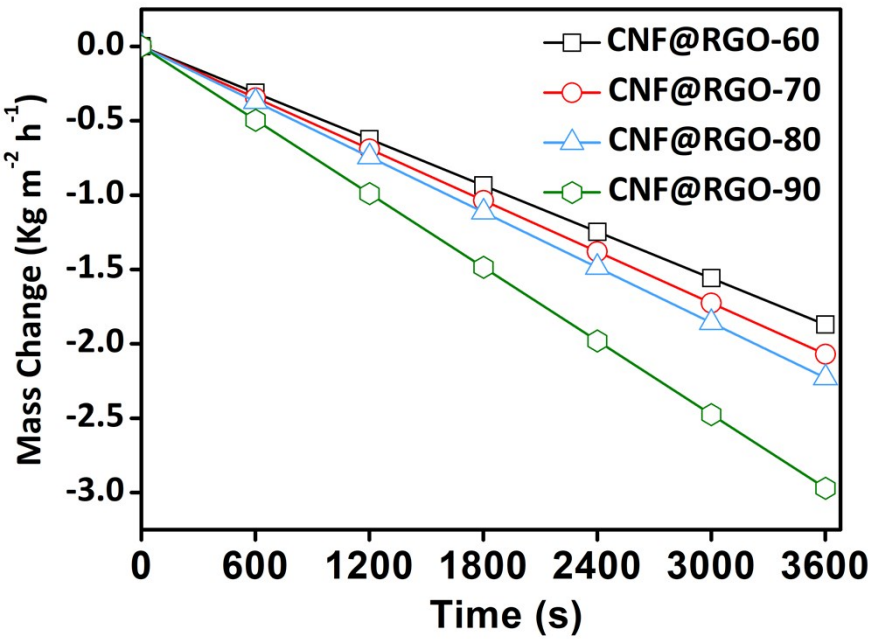

Figure S19. The evaporation rate of **CNF@RGO-*n*** under 2 suns at ~25 °C and a relative humidity of 50-55%.

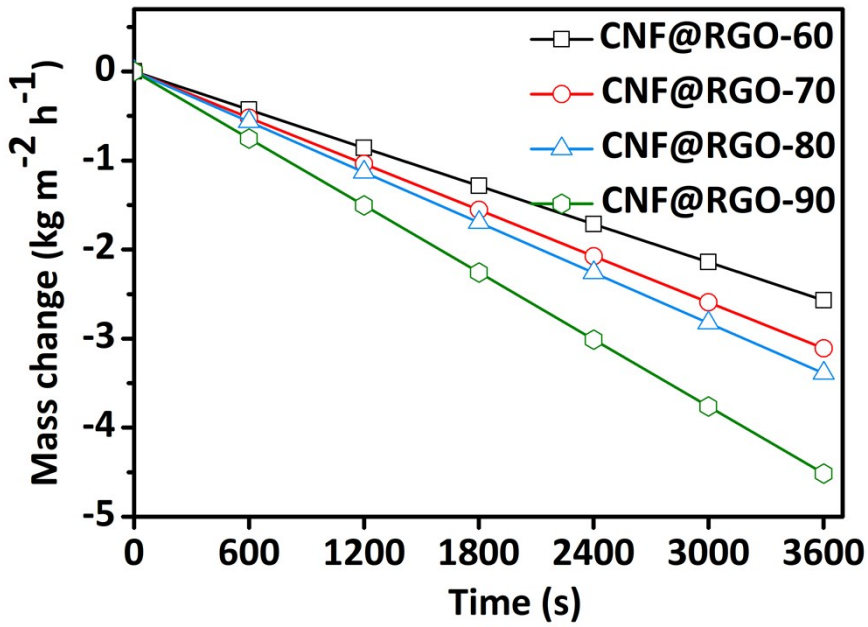

Figure S20. The evaporation rate of **CNF@RGO-*n*** under 3suns at ~25 °C and a relative humidity of 50-55%.

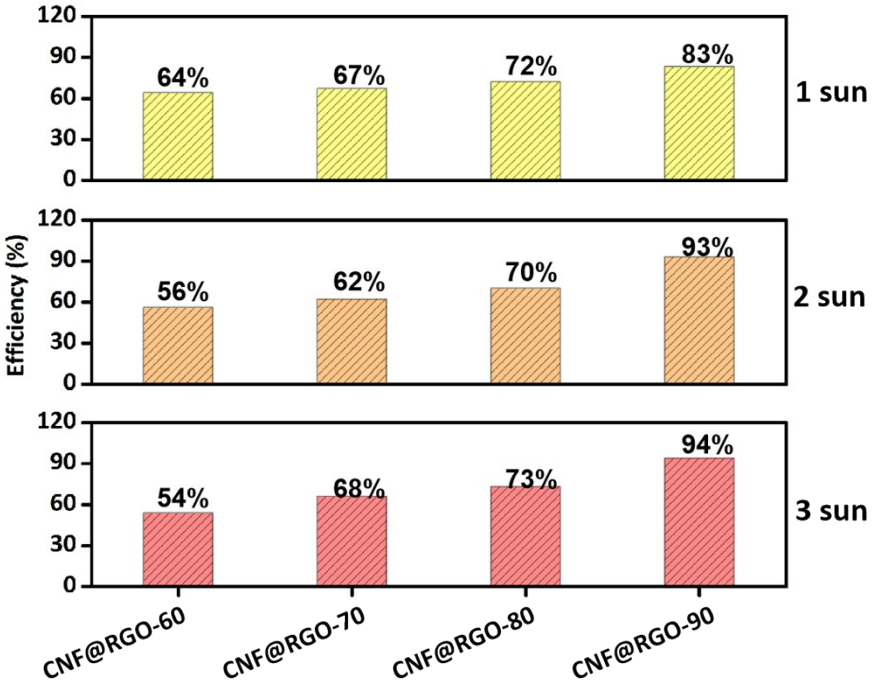

Figure S21 The efficiency of **CNF@RGO-60，70，80，90** under 1, 2, 3 sun.

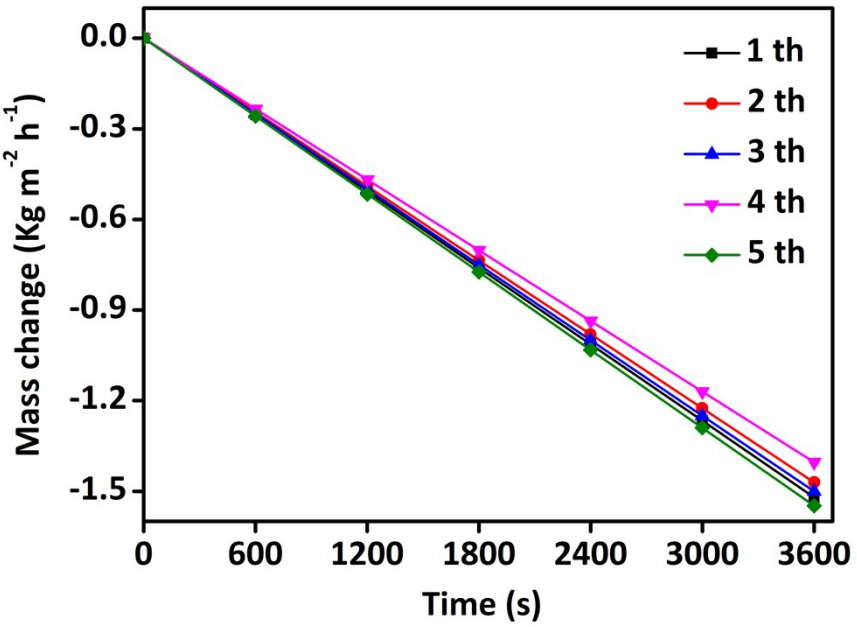

Figure S22. The evaporation rate of 5 cycles of **CNF@RGO-90** under 1sun at ~25 °C and a relative humidity of 50-55%.

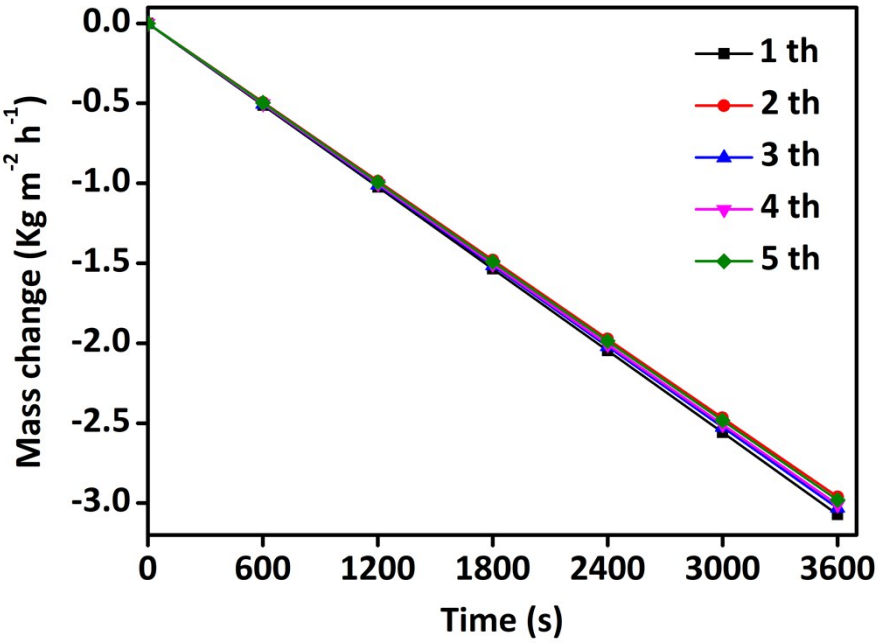

Figure S23. The evaporation rate of 5 cycles of **CNF@RGO-90** under 2suns at ~25 ^{o}C and a relative humidity of 50-55%.

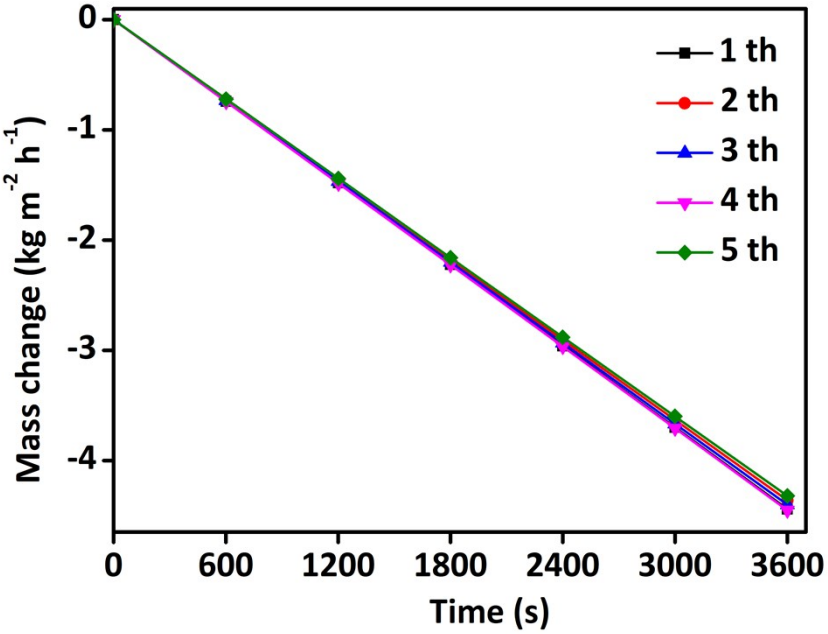

Figure S24. The evaporation rate of 5 cycles of **CNF@RGO-90** under 3 suns at ~25 ^{o}C and a relative humidity of 50-55%.

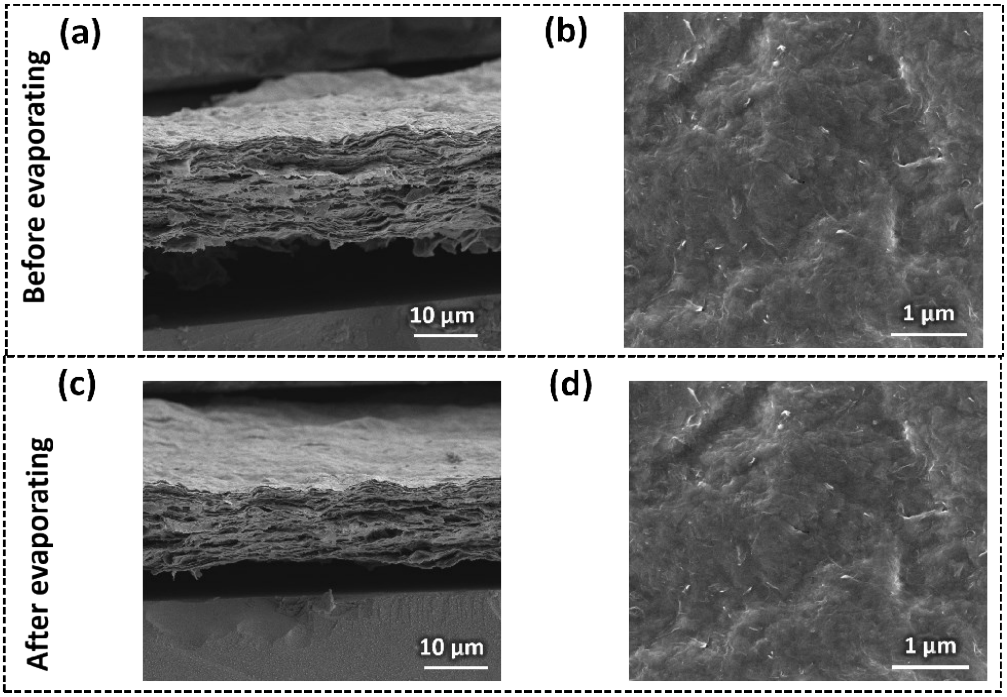

Figure S25. The SEM images of **CNF@RGO-60**. (a,b) The images of cross-section and surface before evaporation. (c,d) The images of cross-section and surface after evaporating under 1 sun over 5 hours.

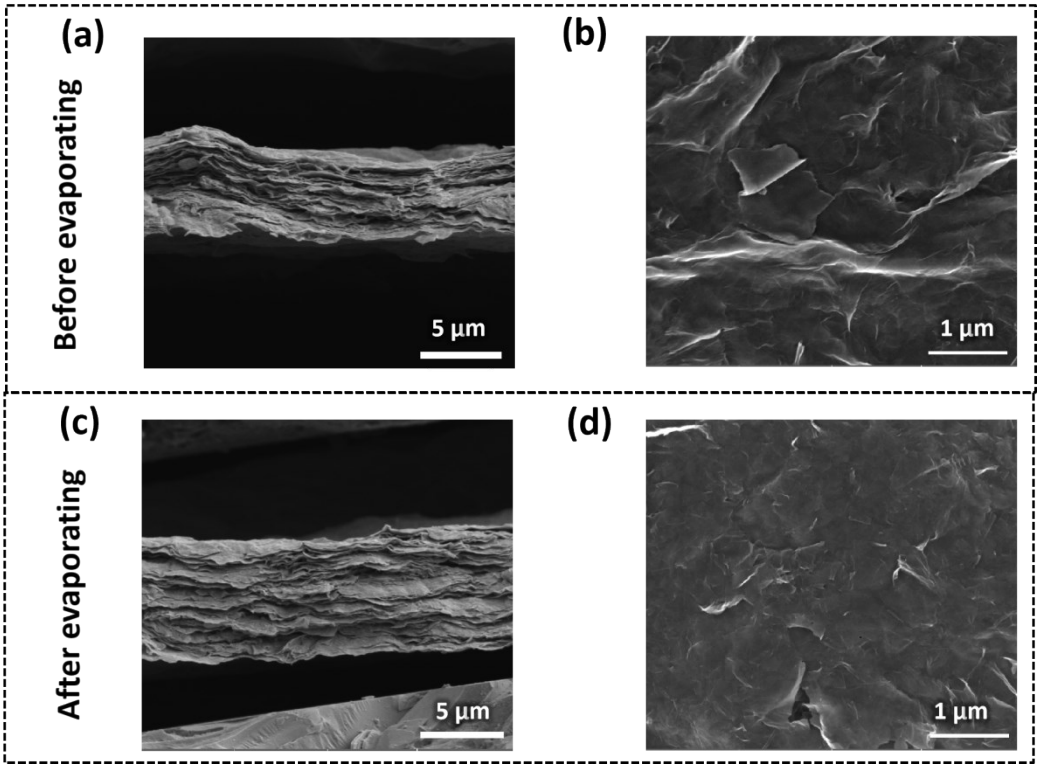

Figure S26. The SEM images of **CNF@RGO-70**. (a,b) The images of cross-section and surface before evaporation. (c,d) The images of cross-section and surface after evaporating under 1 sun over 5 hours.

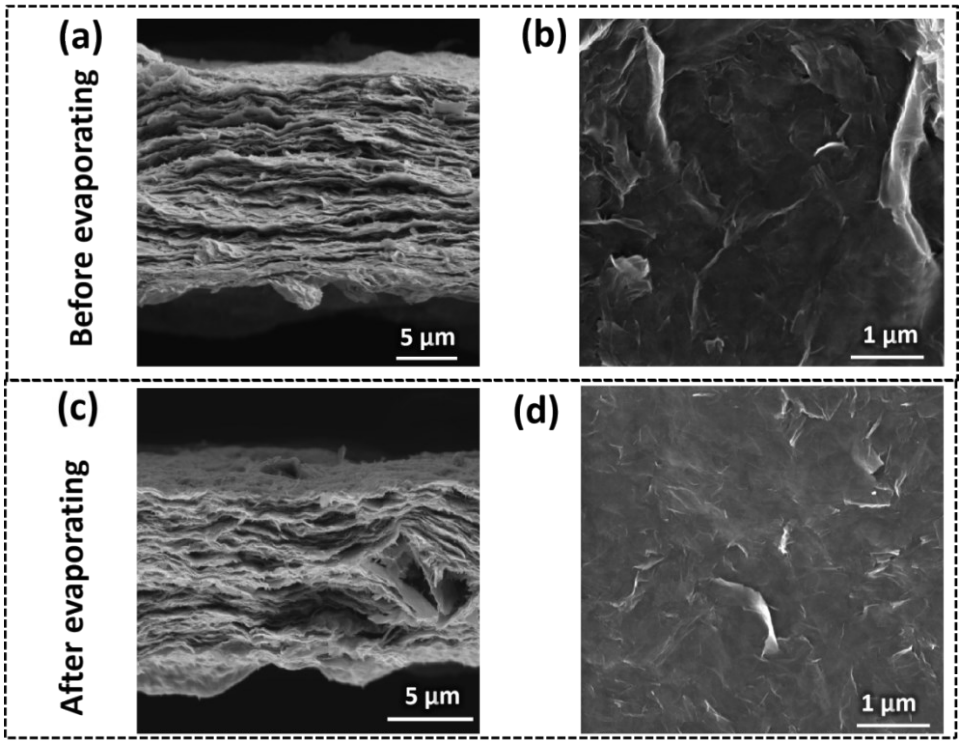

Figure S27. The SEM images of **CNF@RGO-80**. (a,b) The images of cross-section and surface before evaporation. (c,d) The images of cross-section and surface after evaporating under 1 sun over 5 hours.

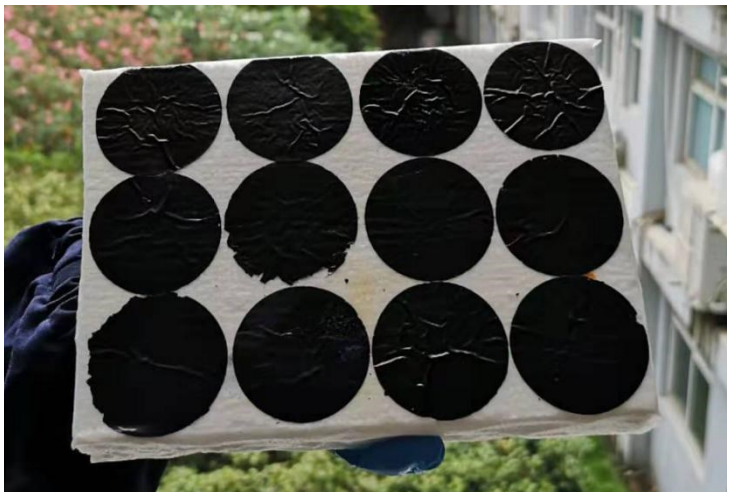

Figure S28. The photograph of an amplified solar steam-generator integrated with 12 unites (total area of **CNF@RGO-90**: ~144 m^2) for evaporating.

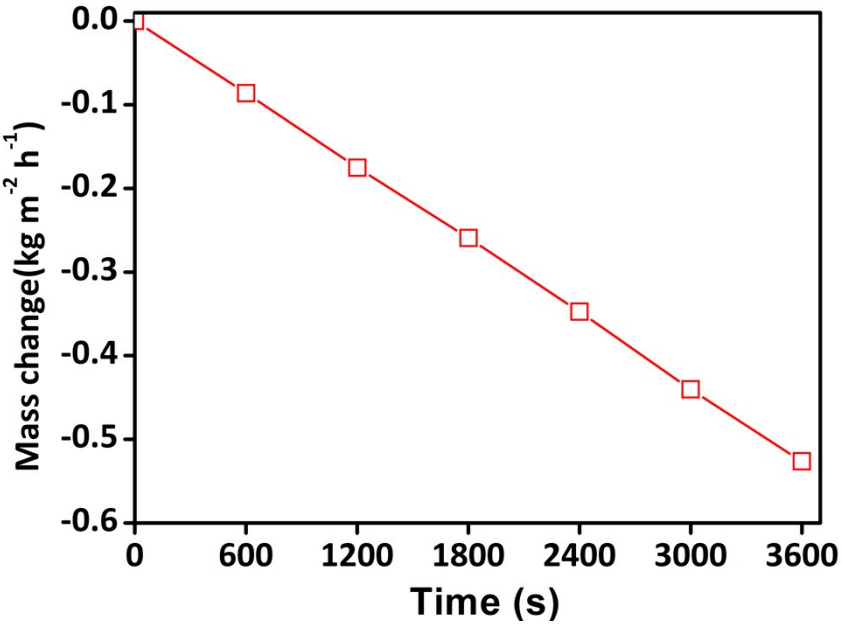

Figure S29. Evaporation rate of **CNF@RGO-n** under 700 kW m^{-2}, under an ambient temperature of 25 °C and relative humidity of 50-55%.

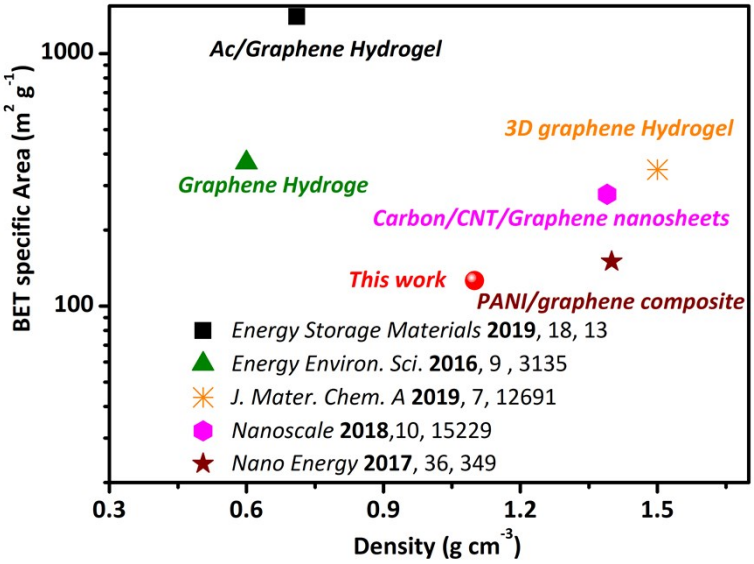

Figure S30. The density and BET specific area of the as-prepared **CNF@RGO-90** and the previously reported graphene-based composites.

Table S1. Solar steam generation performances of different materials. The energy conversion efficiency, and the evaporation rates of various photo-thermal conversion materials under 1 sun.

Sample	Energy conversion (%)	Evaporation rate (kg^{-1} m^{-2} h^{-1})	Ref.
CNT coated wood	65	0.9	*Adv. Mater.* **2017**, 29, 1701756
Porous N-doped graphene	80	1.5	*Adv. Mater.* **2015**, 27, 430
Black Ag particle	95	1.4	*Nano Lett.* **2019**, 19, 1400-407
Hierarchical graphene foam	91	1.4	*Adv. Mater.* **2017**, 29, 1702590
CNT-modified filter paper	75	1.15	*Energy Environ. Sci.* **2017**, 10, 1923
Graphene coated wood	80	1.15	*Adv. Funct. Mater.* 2018, 28, 1707134
Flamed-treated wood	72	1.05	*ACS Appl. Mater. Interfaces* **2017**, 9, 15052
Carbonized rice straw	75	1.2	*ACS Appl. Mater. Interfaces* **2019**,11, 10672-10679
CNT-macroporous silica	82	1.31	*ACS Sustainable Chem. Eng.* **2016**, 4, 1223
Nitrogen-enriched carbon sponge	85	1.31	*Adv. Energy Mater.* **2018**, 8, 1702149
Carbonized daikon	85	1.57	*Adv. Energy Mater.* **2018**, 8, 1702149.
Hollow-CNTs-Aerogels	86	1.44	*Energy Mater Sol. Cells* **2019**, 191, 83.
PPy membrane	82	1.41	*Adv. Energy Mater.* **2019**, 9, 1802158
Carbon nanotubes (CNTs)/wood membrane	65	0.95	*Adv. Energy Mater.* **2018**, 8, 1702884
multilayer PPy nanosheets	92	1.38	*Adv. Mater.* **2019**, *31*, 1807716
Gold nanoparticles coated anodic aluminum oxide membrane	63	1.0	*Sci. Adv.* **2016**, 2, 1501227
CNF@RGO-90	83	1.47	This work

Table S2. The thermal conductivity of previously Reported Nano-carbon composite

Sample	Preparation method	Thermal conductivity	Ref.
Monolayer graphene	Chemical vapor deposition	5000 W/mK	*Nano Lett.* **2010**, *10*, 1645.
expanded graphite film	Annealing 800 °C for 1min, compression 20MP for 5 min	In-plan: 854 W/mK	Carbon **2019**, 153, 565-,574
Porous Graphene film	Chemical vapor deposition	In-plan: 400 W/mK at room temperature	*Adv. Mater.* **201**5, *27*, 4302–4307
Graphene paper	Ball milling in NMP (6 h), annealing at 2850 °C (2 h), mechanical compression (30 MPa)	In-plan: 1529 W/mK at room temperature	Adv. Funct. Mater. **2017**, 27, 1700240
Au Nano-particle decorated graphene film	Sonication in PEI/water (1 h), annealing at 340 °C (2 h), mechanical compression (100 psi, 1 h)	In-plan: 200 W/mK	ACS Appl. Mater. Interfaces **2011**, 3, 1325−1332
G-Graphene film	Sonication in nitric acid and sulfuric acid (72 h), annealing at 1060 °C (2 h)	In-plan: 220 W/mK at room temperature	ACS Appl. Mater. Interfaces **2014**, 6, 15026−15032.
RGO films	GO film was fabricated by 3D print,annealing at 1000 K and gradually Joule-heated to 2000 K or 3000 K .	In-plan: 118 W/mK at room temperature	*Adv. Funct. Mater.* **2019**, *29*, 1901388
Graphite/Copper composites	Mixing the powder of Copper and Graphite for 6 h, heat compression under 900°C, 75 Mpa..	In-plan: 456 W/mK at room temperature	*Carbon* **2019**, 149, 152-164
CNF@RGO-90	Filtration-assisted self-assembly: sonication in water at 80 °C (5h), and filtration fabrication	In-plan: 614-1238 W/mK within 25-80°C	This work

Table S3. The densities and specific surface areas of the previously reported compact nanocarbon-based materials in comparison with the as-prepared compact thin films.

Sample	Density ($g\ cm^{-3}$)	Specifial area ($m^2\ g^{-1}$)	Performance[a]	Ref.
Ac/Graphene Hydrogel	0.71	1402	98 Wh L^{-1}	*Energy Storage Materials* **2019**, 18, 13
Graphene Hydrogel	0.6-1.6	370-1000	65Wh L^{-1}	*Energy Environ. Sci.* **2016**, 9 , 3135
High-density Holey Graphite Nanosheets	0.7-1.6	287-370	384 F cm^{-3}	*Nanoscale Horiz.* **2019**, 4, 526
3D graphene Hydrogel	1.5	347	165 F cm^{-3}	*J. Mater. Chem. A* **2019**, 7, 12691
PSS:PEDOT/graphene film	1.25-0.7	---	203 F cm^{-3}	*Energy Environ. Sci*. **2018**, 11, 559
CNT/Polyaniline Hydrogel	1.19	---	632 F cm^{-3}	*ACS Appl. Mater. Interfaces* **2016**, 8, 34027
Organic molecules/graphene network	1.38	---	633Fcm^{-3}/41 Wh L^{-1}	*J. Mater. Chem. A* **2020**, 8, 461
Porous carbon/ CNT/Graphene nanosheets	1.39	277	877 F cm^{-3}/27.51 WhL^{-1}	Nanoscale **2018**,10, 15229
PANI/graphene composite	1.4	150	650 F cm^{-3} / 44WhL^{-1}	*Nano Energy* **2017**, 36, 349
High Density Porous Graphene Macroform	1.05	---	141 mA h cm^{-3}	*Adv. Energy Mater.* **2018**, 8, 1702395
CNF@RGO-*n*	0.9-1.6	40-126	1238 W /mK, 1.47 kg m^{-2} h^{-1}	This work

[a] The previously reported compact carbon composites were mainly used as the electrode materials for energy storage, associated with their high electric conductivities. While, the as-prepare compact thin films exhibit a dual-role function of thermal management and water pumping, as demonstrated by their excellent performance in solar-steam generation.